eScience 2 (2022) 110–115

Contents lists available at ScienceDirect

eScience

journal homepage: www.keaipublishing.com/en/journals/escience

Research Paper

Effect of electrolyte anions on the cycle life of a polymer electrode in aqueous batteries

Ye Zhang [a,b], Lihong Zhao [a,b], Yanliang Liang [a,b], Xiaojun Wang [a,b], Yan Yao [a,b,*]

[a] Department of Electrical and Computer Engineering, Materials Science and Engineering Program, University of Houston, Houston, TX, 77204, USA
[b] Texas Center for Superconductivity at the University of Houston, Houston, TX, 77204, USA

HIGHLIGHTS

- The effect of anions of zinc salts in aqueous electrolytes on the longevity of a p-dopable polymer was investigated.
- The volume change of the polymer electrode induces mechanical fracture, leading to its capacity loss.
- Anions with lower solvation degree induce less volume change, thus yielding long-term cycling.

GRAPHICAL ABSTRACT

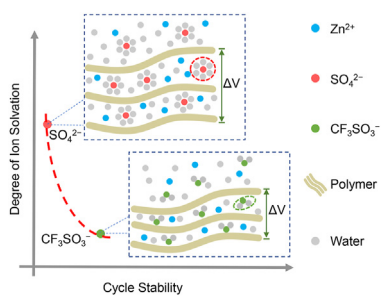

ARTICLE INFO

Keywords:
Aqueous batteries
Polymer electrode
Anions
Volume change

ABSTRACT

Redox polymers are a class of high-capacity, low-cost electrode materials for electrochemical energy storage, but the mechanisms governing their cycling stability are not well understood. Here we investigate the effect of anions on the longevity of a *p*-dopable polymer through comparing two aqueous zinc-based electrolytes. Galvanostatic cycling studies reveal the polymer has better capacity retention in the presence of triflate anions than that with sulfate anions. Based on electrode microstructural analysis and evolution profiles of the cell stacking pressure, the origin of capacity decay is ascribed to mechanical fractures induced by volume change of the polymer active materials during repeated cycling. The volume change of the polymer with the triflate anion is 61% less than that with the sulfate anion, resulting in fewer cracks in the electrodes. The difference is related to the different anion solvation structures—the triflate anion has fewer solvated water molecules compared with the sulfate anion, leading to smaller volume expansion. This work highlights that anions with low solvation degree are preferable for long-term cycling.

1. Introduction

The global need for energy storage is prompting the development of low-cost, long-lasting energy storage devices [1,2]. Considering the sheer scale of the demand, it is critical to use energy storage materials that are made of earth-abundant elements and can be synthesized with environmentally friendly chemistries [3–5]. Among the various candidates, redox polymers composed of abundant elements (C, H, and O) and manufactured using low-carbon-emission processes have demonstrated unique advantages in terms of sustainability [1,3,6–9]. Interestingly, the storage capability of redox polymers is not constrained by the type of counter-ion. To balance the charge, anions, cations, or both can be

* Corresponding author.
E-mail address: yyao4@uh.edu (Y. Yao).

https://doi.org/10.1016/j.esci.2022.01.002
Received 8 November 2021; Received in revised form 31 December 2021; Accepted 27 January 2022
Available online 2 February 2022

utilized, allowing redox polymers to be used in a variety of applications, such as multivalent and dual-ion batteries and supercapacitors [4,10,11].

Cycle life is a key figure of merit for any battery technology. Redox polymers typically show better longevity than small molecule-based organic electrodes, because the former dissolve less readily in liquid electrolytes [6]. While a few studies have recognized the effect of electrolytes on the cycle life of redox polymer electrodes, a mechanistic understanding is still lacking. For example, Luo et al. investigated the anion effect on the redox potential and cycling stability of Zn-organic radical batteries, but the detailed mechanism was not explored [12]. Xie et al. observed a similar trend of electrolyte-dependent longevity for a new redox polymer, poly(2,3-dithiino-1,4-benzoquinone), but again, the origin of the anion effect was not discussed [13]. A fundamental understanding is therefore required to correlate the charge storage mechanism and cycle life of polymer batteries.

Previously, using electrochemical quartz crystal microbalance with dissipation monitoring (EQCM-D) and in situ Fourier transform infrared spectroscopy (FTIR), we discovered mixed Zn^{2+} cation and anion storage in a quinone polymer [14]. Recently, Nimkar et al. reported an EQCM-D study of polyimides and highlighted the pronounced effect of water co-insertion with cations [15]. Both studies shed light on the reaction mechanism, but neither work established the correlation between mechanism and cycle life performance.

In this work, we investigate the effects of anions on the cycle life of a *p*-dopable polymer, poly(benzoquinonyl sulfide) (PBQS). When using $Zn(CF_3SO_3)_2$-based electrolyte, PBQS shows better capacity retention compared with $ZnSO_4$-based electrolyte. Based on analysis of the electrode's microstructure and evolution profiles of the cell stacking pressure, we identify mechanical fracture of the electrodes as the origin of capacity decay in redox polymer electrodes. The electrode with $Zn(CF_3SO_3)_2$-based electrolyte shows 61% less volume change and fewer cracks than those using the $ZnSO_4$-based electrolyte. In situ FTIR studies further reveal that the degree of volume change correlates to the anion solvation structures. Although PBQS shows a mixed electrochemical storage mechanism involving both Zn^{2+} and the anion within the respective voltage range, we show that the anion plays the dominant role in the cycle life of the PBQS-Zn battery.

2. Materials and methods

2.1. Materials

Zinc trifluoromethanesulfonate ($Zn(CF_3SO_3)_2$, 98%) and deuterium oxide (D_2O, 99.9 at% D) were purchased from Millipore Sigma. Zinc sulfate heptahydrate ($ZnSO_4{\cdot}7H_2O$, > 99%) and zinc foil (99.9%) were obtained from Fisher Scientific. Glass fiber (150 μm) and polypropylene separator (20 μm, model 3501, Celgard) were obtained from Whatman and Celgard, respectively. Ketjenblack carbon (AkzoNobel) and polytetrafluoroethylene (PTFE, MTI) were used during electrode fabrication. All reagents were used as received from industrial vendors.

2.2. Electrochemical measurement

PBQS was synthesized following a method reported in the literature [16]. To prepare composite electrodes, PBQS, Ketjenblack carbon (KB), and PTFE were mixed in a mass ratio of 7:2:1 with the aid of ethanol. Freestanding electrodes were then cut into small pieces and dried at 80 °C under vacuum for 12 h. The areal loading of the active material was ~2 mg cm^{-2} unless otherwise indicated. The electrochemical performance of the composite electrodes was evaluated in 2032 coin-type cells using glass fiber as the separator, zinc foil as the anode, and 1 M $ZnSO_4$ or 1 M $Zn(CF_3SO_3)_2$ aqueous solutions as the electrolytes. Electrochemical characterizations were performed with a potentiostat (VMP3, Biologic).

2.3. In situ monitoring of stacking pressure

The stacking pressure's evolution during electrochemical tests was monitored in a PEEK split cell, illustrated in Fig. 2a. Cell components were sandwiched between two titanium rods serving as current collectors. Two rigid stainless-steel plates were used to maintain a constant gap in the cell, with an initial stacking pressure of 6 psi. A force sensor (AT8103, AUTODA) was placed between the titanium rod and the stainless-steel plate. The force sensor had a sensitivity limit of 0.015 N, which corresponded to ~0.02 psi when the electrode area was considered. The loading of PBQS was increased to 10 mg cm^{-2} in these tests. During cell assemblage, 200 μL of electrolyte was added and a polypropylene separator (20 μm) was used to minimize volume change from the separator. In the split cell setup used here for pressure monitoring, the seal applied by vacuum grease was not meant to be perfect, and we didn't observe gas buildup due to H_2 generation as we would usually observe in the case of coin cells, where better sealing is expected. The possible reason is that the generated H_2 gas easily escaped from the gaps in the split cells. The cells were cycled in the voltage range of 0.5–1.6 V at a current density of 40 mA g^{-1} (0.2 C).

2.4. In situ FTIR measurement

In situ FTIR spectroscopy was performed using a spectrometer (Nicolet iS5, Thermo Scientific) with an attenuated total reflection accessory. The mass ratio of the composite electrode was changed to 8:1:1 to improve the signals for PBQS. Fig. S1 shows the schematics of the set-up. The electrode was pressed against a diamond window, followed by stainless-steel mesh serving as the current collector, glass fiber as the separator, and zinc foil as the anode. To avoid complications from overlapping absorption bands of O–H and C═O, D_2O was used as the electrolyte solvent. The cell was tested under a current of 400 mA g^{-1}, with FTIR spectra collected every minute. To visualize the evolution of the FTIR spectra, the absorbances were plotted against time as two-dimensional color maps. To evaluate the correlation between FTIR signals, the correlation coefficient (r) between two data sets (x and y) was calculated using Eq. (1) [17]:

$$r = \frac{\sum (x-\bar{x})(y-\bar{y})}{\sqrt{\sum (x-\bar{x})^2 \sum (y-\bar{y})^2}} \tag{1}$$

where $\bar{x}$ and $\bar{y}$ are the mean values. A correlation coefficient close to 1 indicates x and y have a strong correlation, whereas a correlation coefficient close to 0 means x and y have a weak or no correlation.

2.5. Microstructural analysis of composite cathodes

Cross-sections of PBQS electrodes were prepared using an argon-ion beam cross-section polisher (IB-19520CCP, JEOL). The cycled electrodes were washed with deionized water and ethanol to remove residual electrolyte and dried at room temperature under vacuum overnight. To minimize artifacts and prevent heat damage, an accelerating voltage of 4 kV and a milling rate ~25 μm h^{-1} were used, and samples were cooled with liquid nitrogen during the milling process.

Scanning electron microscope (SEM) measurements were conducted using an FEI XL-30 FEG at 5 kV. Image segmentation was carried out with ImageJ software using the threshold method. PBQS particles were identified and segmented by threshold values before the original grayscale image was converted to binary. The areas of each particle were then counted by the software. The areas of particles before and after cycling were compared using a *t*-test with a significance value of $p < 0.05$.

3. Results and discussion

To study the effect of anions on the cycling performance of polymer electrodes, PBQS-Zn cells were assembled and separately tested in 1 M $ZnSO_4$ and $Zn(CF_3SO_3)_2$ electrolytes. Figs. 1a and b shows selected voltage profiles under a current density of 400 mA g^{-1}. Both cells delivered an initial discharge capacity of ~230 mAh g^{-1}. Little change in the shape of the voltage profiles over cycles indicated a reversible charge storage process. The cell tested in 1 M $Zn(CF_3SO_3)_2$ electrolyte showed a better discharge capacity retention of 78% after 200 cycles compared with in $ZnSO_4$-based electrolyte (63%, Fig. 1c). A comparable difference in capacity retention was maintained when cells were tested at different rates (Fig. S2).

To investigate the origin of capacity decay, cycled electrodes were polished to expose their cross-sections for SEM imaging. In the pristine electrode (Fig. 1d), micron-sized PBQS particles were embedded in a porous network of carbon and binder. Analysis of its segmented binary image (Fig. 1e) showed the average domain size of the PBQS particles to be 1.23 μm^2 (Table S1). More than 70% of the total domain area was composed of particles smaller than 5 μm^2 (Fig. 1f). After 100 cycles in 1 M $ZnSO_4$ electrolyte, apparent cracks were observed (Fig. 1g), especially along the edge of larger PBQS particles; the cracks were attributed to repeated expansion−contraction during the electrochemical process. The formation of these gaps led to the loss of electric contact between redox active particles and the carbon network, explaining the capacity decay during cycling. Analysis of the electrode microstructure (Fig. 1h) showed the polymer had an average particle domain of 2.04 μm^2, which was 65% larger than in the pristine sample (Table S1). The difference in domain area is statistically significant, as verified by a *t*-test (Supporting Information) [18]. After cycling in $ZnSO_4$, the area fraction for particles < 1 μm^2 was smaller than in pristine PBQS, while the value for particles > 11 μm^2 was much larger. There are two possible reasons for the particle domain increase: (i) polymer conformation expansion due to repeated ion insertion–extraction, and (ii) salts and solvent molecules becoming trapped in the polymer matrix [19–21]. Since any neutral species were removed by washing and drying the electrodes before polishing, the particle domain increase was a result of repeated ion storage. In contrast, the electrode cycled in 1 M $Zn(CF_3SO_3)_2$ electrolyte had a moderate PBQS domain size of 1.52 μm^2 (Figs. 1j–l), which was an increase from the pristine PBQS particles (Fig. 1f) but much smaller than that of PBQS cycled in 1 M $ZnSO_4$ electrolyte. More importantly, no obvious cracks were observed on the electrode cross-section, and the particles and carbon were in good contact, which explained the better capacity retention obtained in the $Zn(CF_3SO_3)_2$ electrolyte. These observations suggest

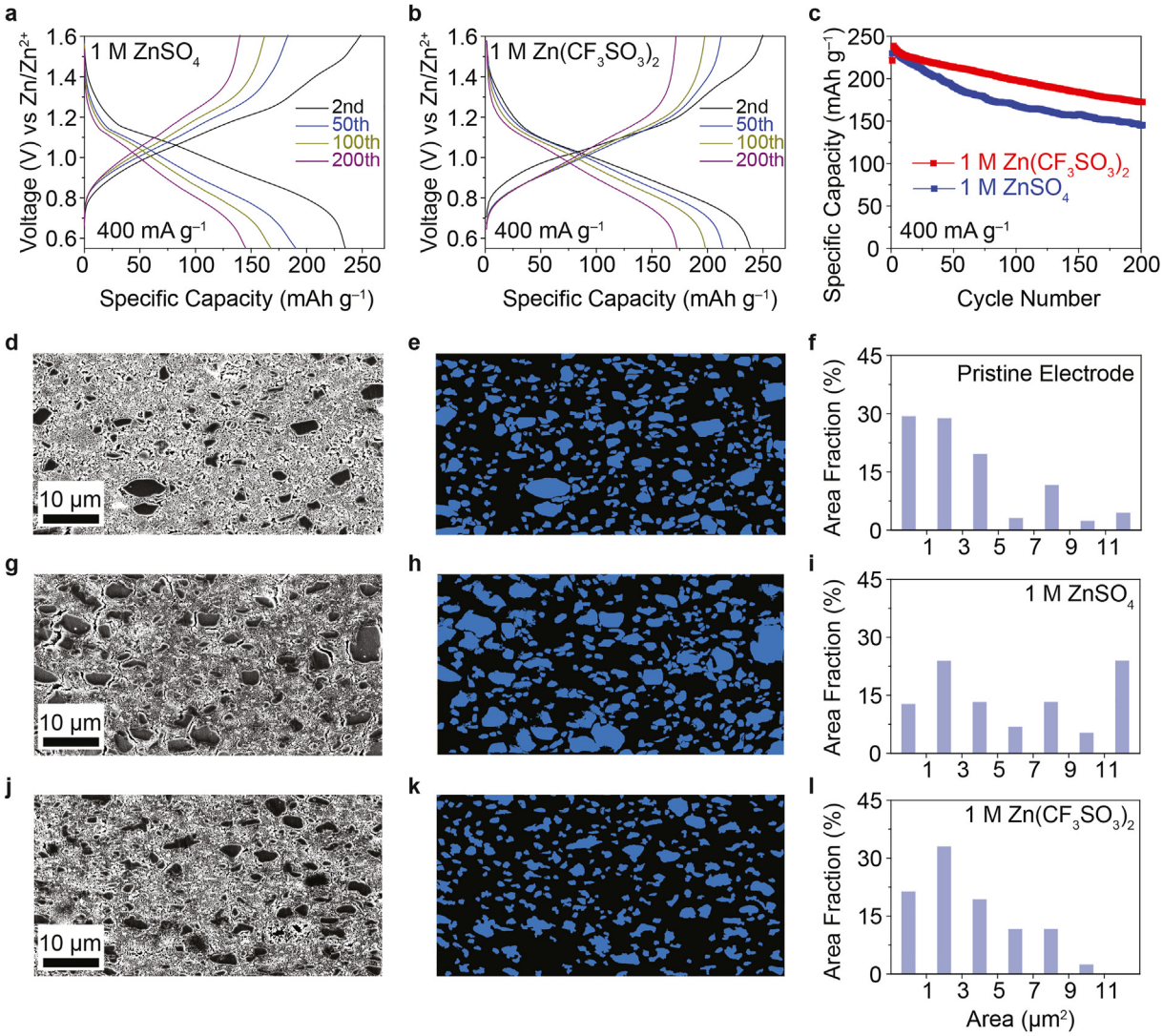

Fig. 1. Electrochemical performance and microstructural analysis. Voltage profiles of selected cycles for PBQS-Zn cells tested in (a) 1 M $ZnSO_4$ and (b) 1 M $Zn(CF_3SO_3)_2$ electrolytes. (c) Capacity retention for 200 cycles. Cross-sectional SEM images, segmented binary images, and area fraction distributions of PBQS particles (d–f) in the pristine state, (g–i) after 100 cycles in 1 M $ZnSO_4$, and (j–l) after 100 cycles in 1 M $Zn(CF_3SO_3)_2$.

crack formation was the root cause of the capacity decay, driven by the particle volume change during cycling. The choice of anion species resulted in different degrees of particle size change, as PBQS tested in the $Zn(CF_3SO_3)_2$ electrolyte showed a smaller size increase, leading to better cell performance.

To investigate polymer volume change during the electrochemical cycling process, PBQS electrodes were tested in split cells using zinc foils as the anode (Figs. 2a and d). The distance between titanium rods was fixed with stainless-steel plates and screws so that the electrode volume expansion could be reflected by changes in the stacking pressure, recorded by a force sensor. Considering the volume change of zinc metal (3.4×10^{-4} cm^3 with 2 mAh capacity) was negligible compared to the volume of the PBQS electrode (~3×10^{-2} cm^3), the change in stacking pressure was mainly attributed to volume change in the PBQS cathode. Fig. 2b shows the voltage profile (black line) and pressure change (blue line) for a PBQS-Zn cell tested in 1 M $ZnSO_4$ electrolyte. The cell delivered a reversible capacity of 220 mAh g^{-1} (Fig. S3a), agreeing with our previous report [14]. The pressure gradually increased with cycling, indicating a net expansion of the polymer volume after each cycle. This phenomenon can be explained by solvents and salts becoming trapped in the polymer matrix during the cycling process [19–21].

A closer look at the second cycle in Fig. 2b reveals that the polymer electrode expanded during the discharge process as cell pressure increased. Upon charging, the pressure increased first, then decreased, suggesting multiple charge carriers participated in the reaction. Our previous study revealed that PBQS shows mixed Zn^{2+} and anion storage via its carbonyl and thioether groups, respectively [14]. The *p*-doping process started at ~1.1 V and above, showing an additional voltage plateau at ~1.4 V. Below 1.1 V, the charge storage was dominated by the *n*-doping process (Fig. S4). During the *p*-doping of thioether groups, anions diffused into the polymer matrix to compensate for the charge. Therefore, the significant pressure increase during charging was caused by an influx of SO_4^{2-}. The pressure effect can be clearly seen by separating the contributions from cation and anion, as presented in Fig. S5. Fig. 2c shows the pressure variation in each cycle, with an average value of ~9 psi.

When 1 M $Zn(CF_3SO_3)_2$ was used as the electrolyte, the cell delivered a similar reversible capacity (Fig. S3b) and pressure profile (Fig. 2e), but a reduced pressure variation of 3.5 psi on average (Fig. 2f), which was 61% less than in the sulfate-based electrolyte. The relatively larger pressure change in the first cycle resulted from a greater pressure increase in the discharge process due to Zn^{2+} influx. In later discharge processes, a similar pressure increase was partially canceled out by anion outflux, resulting in a relatively small volume change. These differences in pressure change in the two electrolytes agree with cross-sectional observations that sulfate induced a larger volume change in the polymer particles.

To discover the reason for the difference in polymer volume change with different anions, in situ FTIR studies were performed in both electrolytes. FTIR spectra for PBQS-Zn cells with detailed signal assignments are shown in Fig. S6 and Table S2, where the signals of S–O (SO_4^{2-} or $CF_3SO_3^-$), carbonyl groups (C═O and C–O), and solvent (O–D) can be clearly distinguished. Fig. 3b shows the evolution of functional groups over time (Fig. 3a) in 1 M $ZnSO_4$ electrolyte. The periodic diminishment and reappearance of C═O (~1631 cm^{-1}) and C–O (~1400 cm^{-1}) suggest the carbonyl groups were the redox centers in the electrochemical reaction. During the first charging of PBQS, the signal of SO_4^{2-} (S–O, ~1100 cm^{-1}) increased significantly, which agrees with the increase in stacking pressure during the same stage (Fig. 2b), indicating volume expansion was mainly caused by anion insertion. Moreover, the signal from the solvent molecule (O–D, ~2300 cm^{-1}) showed the same trend with SO_4^{2-} during the charging process. The correlation between S–O and O–D bonds was quantitatively determined by analyzing their signal changes, as shown in Fig. 3c. A correlation coefficient of 0.75 was obtained, indicating a strong correlation between S–O and O–D [17]. Therefore, the SO_4^{2-} anion was stored in its solvated form in the polymer, resulting in significant electrode volume expansion.

The FTIR spectra collected in 1 M $Zn(CF_3SO_3)_2$ electrolyte showed similar trends in terms of the change in carbonyl groups during cycling (Figs. 3d and e). However, while the strengthening and diminishment of anion signals (S–O, ~1000 cm^{-1}) is evident in Fig. 3f, the signal change for the solvent (O–D) is not obvious. The correlation coefficient was calculated to be 0.43, indicating the correlation between $CF_3SO_3^-$ and D_2O was weaker, so the $CF_3SO_3^-$ anion was less solvated than SO_4^{2-} when stored in the polymer, resulting in less electrode volume change, as shown in Figs. 2e and f.

The differences in the two anions' solvation structures can be explained by their affinity toward water molecules. The attractive force ($F(r)$) between an ion and a polar molecule at a distance of r can be calculated with Eq. (2)

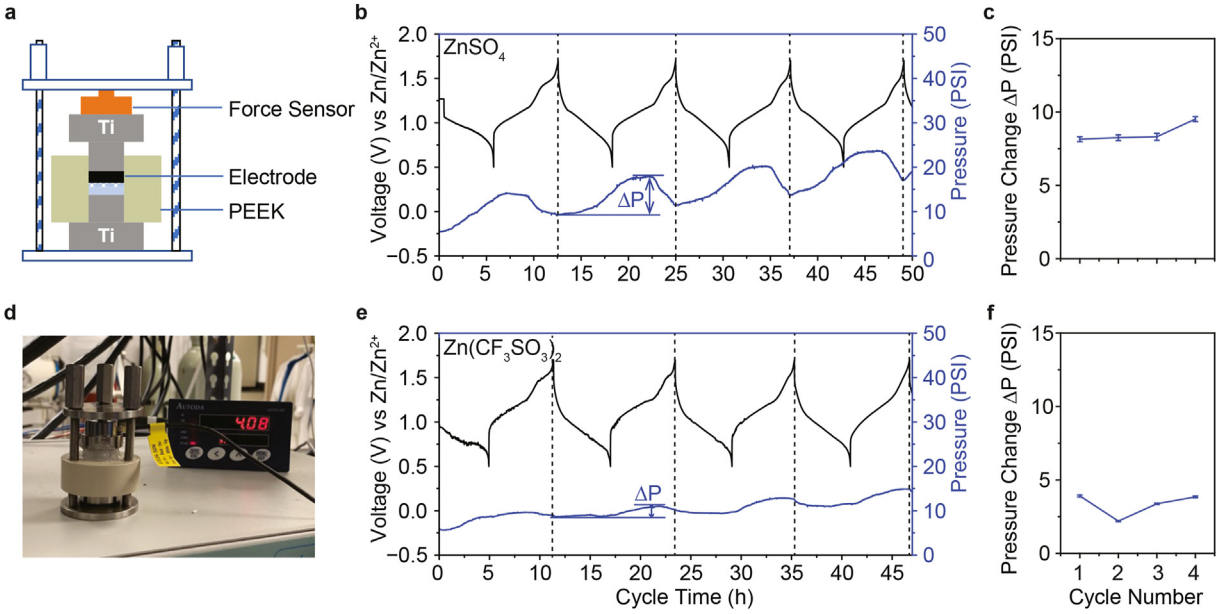

Fig. 2. In situ monitoring of stacking pressure. (a) Schematic illustration and (d) photograph of the cell configuration for pressure monitoring. Voltage and pressure evolution profiles in (b) 1 M $ZnSO_4$ and (e) 1 M $Zn(CF_3SO_3)_2$ electrolytes. The net pressure changes are shown in (c) and (f).

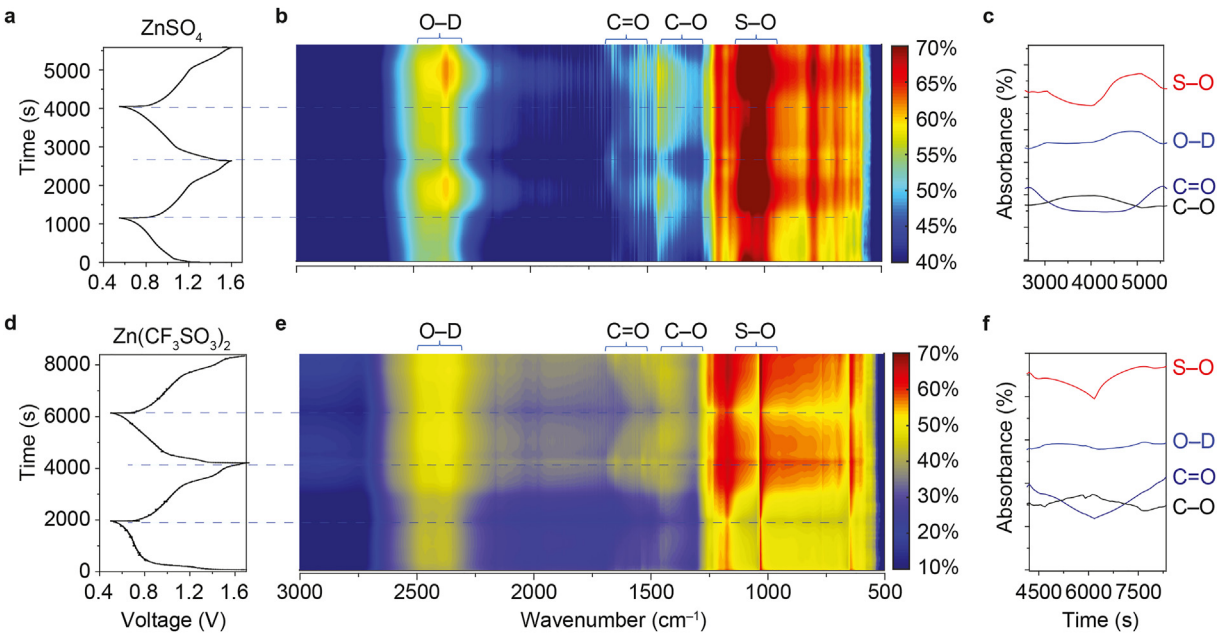

Fig. 3. In situ FTIR measurements. Voltage profiles of PBQS-Zn cells tested in (a) 1 M $ZnSO_4$ and (d) 1 M $Zn(CF_3SO_3)_2$ electrolytes. Two-dimensional color map of the FTIR spectra obtained in (b) 1 M $ZnSO_4$ and (e) 1 M $Zn(CF_3SO_3)_2$ electrolytes. The color bar represents FTIR absorbance. The time-dependent absorbances of selected functional groups during the second cycle are plotted in (c) and (f). Peak assignments can be found in Fig. S6 and Table S2.

$$F(r) = -2\alpha(ze)^2/(4\pi\varepsilon_0\varepsilon)^2 r^5 \quad (2)$$

where α is the polarizability of the molecule, z is the valence of the ion, e is the elementary charge, ε_0 is the absolute dielectric constant under vacuum, and ε is the dielectric constant of the media [22]. At a given distance r, the divalent SO_4^{2-} has a stronger electrostatic attraction toward polar molecules than monovalent $CF_3SO_3^-$ does, resulting in a higher degree of solvation. These hypotheses are supported by previous DFT calculations and vibrational spectroscopy studies indicating that SO_4^{2-} is closely bonded with six water molecules [23,24], whereas the coordination number for $CF_3SO_3^-$ is less than three [25–27].

The difference in anion-induced volume change in the two electrolytes highlights anion hydrophilicity as a determining factor for the cycle life of *p*-dopable polymers. SO_4^{2-} shows a strong attraction to water because of its divalent charge (Fig. 4a). During the charge storage process, the solvated anions induced larger volume change in the polymer matrix (Fig. 4b), leading to electrode fracture and capacity decay. The interaction between the monovalent $CF_3SO_3^-$ and water, on the other hand, was weaker. According to the FTIR analysis, $CF_3SO_3^-$ was exclusively involved in hydrogen bonding at its $-SO_3^-$ end (Fig. 4c) [27]. This reduction in the number of anion solvated water molecules minimized the degree of polymer volume change during the redox process (Fig. 4d). Other strategies to alleviate the effect of electrode volume change include employing concentrated electrolytes with reduced ion solvation [13,28], tuning anion solvation by modifying polymer side chains [29], or constructing nanostructured polymer electrodes to accommodate strain and avoid cracking or fracturing [30–32].

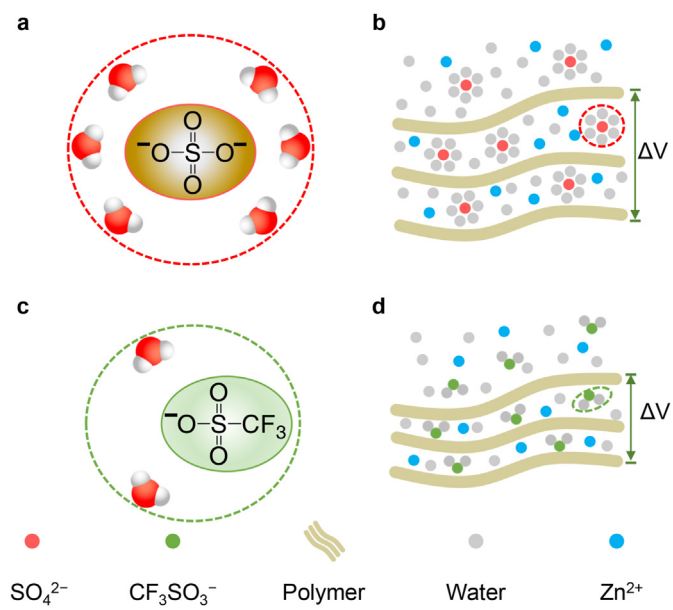

Fig. 4. Schematic of charge storage in polymer electrodes. (a) The sulfate ion is solvated with more water molecules due to its stronger electrostatic attraction toward water, resulting in (b) a larger polymer volume change during the redox process. (c) The triflate ion, solvated with less water, induces (d) a smaller volume change.

4. Conclusions

In summary, we have investigated the influence of anions on the cycling stability of PBQS electrodes in aqueous electrolytes using electrode cross-section microstructural analysis, stacking pressure monitoring, and in situ FTIR spectroscopy. We have identified electrode fracture, arising from polymer volume change during the anion storage process, as a major source of capacity decay. The degree of volume change is influenced by the anion solvation structure in the electrolytes. The divalent SO_4^{2-} solvated with more water molecules induces greater electrode volume change, while $CF_3SO_3^-$ with less hydration cause less volume change, thereby yielding better battery cycling stability. Our work reveals the important correlation between anion solvation and the long-term cycling stability of polymer-based electrode materials.

Author contributions

Y. Yao, Y. L. Liang, and Y. Zhang proposed the concept. Y. Zhang performed the experiments. X. Wang synthesized the PBQS polymer. All authors participated in data analysis and co-wrote the manuscript.

Declaration of competing interest

The authors declare that they have no known competing financial interests or personal relationships that could have appeared to influence the work reported in this paper.

Acknowledgments

Y.Y. acknowledges funding support from the Cullen College Professorship. We thank Bin Wang for his assistance in the FTIR measurements.

Appendix A. Supplementary data

Supplementary data to this article can be found online at https://doi.org/10.1016/j.esci.2022.01.002.

References

[1] D. Larcher, J.M. Tarascon, Towards greener and more sustainable batteries for electrical energy storage, Nat. Chem. 7 (2015) 19–29.
[2] J. Liu, J.-G. Zhang, Z. Yang, J.P. Lemmon, C. Imhoff, G.L. Graff, L. Li, J. Hu, C. Wang, J. Xiao, G. Xia, V.V. Viswanathan, S. Baskaran, V. Sprenkle, X. Li, Y. Shao, B. Schwenzer, Materials science and materials chemistry for large scale electrochemical energy storage: from transportation to electrical grid, Adv. Funct. Mater. 23 (2013) 929–946.
[3] Y. Liang, Y. Yao, Positioning organic electrode materials in the battery landscape, Joule 2 (2018) 1690–1706.
[4] P. Novák, K. Müller, K.S.V. Santhanam, O. Haas, Electrochemically active polymers for rechargeable batteries, Chem. Rev. 97 (1997) 207–282.
[5] Z. Huang, Y. Hou, T. Wang, Y. Zhao, G. Liang, X. Li, Y. Guo, Q. Yang, Z. Chen, Q. Li, L. Ma, J. Fan, C. Zhi, Manipulating anion intercalation enables a high-voltage aqueous dual ion battery, Nat. Commun. 12 (2021) 3106.
[6] P. Poizot, J. Gaubicher, S. Renault, L. Dubois, Y. Liang, Y. Yao, Opportunities and challenges for organic electrodes in electrochemical energy storage, Chem. Rev. 120 (2020) 6490–6557.
[7] S. Muench, A. Wild, C. Friebe, B. Häupler, T. Janoschka, U.S. Schubert, Polymer-based organic batteries, Chem. Rev. 116 (2016) 9438–9484.
[8] Z. Tie, Z. Niu, Design strategies for high-performance aqueous Zn/organic batteries, Angew. Chem. Int. Ed. 59 (2020) 21293–21303.
[9] T.P. Nguyen, A.D. Easley, N. Kang, S. Khan, S.-M. Lim, Y.H. Rezenom, S. Wang, D.K. Tran, J. Fan, R.A. Letteri, X. He, L. Su, C.-H. Yu, J.L. Lutkenhaus, K.L. Wooley, Polypeptide organic radical batteries, Nature 593 (2021) 61–66.
[10] J. Kim, J.H. Kim, K. Ariga, Redox-active polymers for energy storage nanoarchitectonics, Joule 1 (2017) 739–768.
[11] F. Mo, Q. Li, G. Liang, Y. Zhao, D. Wang, Y. Huang, J. Wei, C. Zhi, A self-healing crease-free supramolecular all-polymer supercapacitor, Adv. Sci. 8 (2021) 2100072.
[12] Y. Luo, F. Zheng, L. Liu, K. Lei, X. Hou, G. Xu, H. Meng, J. Shi, F. Li, A high-power aqueous zinc–organic radical battery with tunable operating voltage triggered by selected anions, ChemSusChem 13 (2020) 2239–2244.
[13] J. Xie, F. Yu, J. Zhao, W. Guo, H.-L. Zhang, G. Cui, Q. Zhang, An irreversible electrolyte anion-doping strategy toward a superior aqueous Zn-organic battery, Energy Storage Mater. 33 (2020) 283–289.
[14] Y. Zhang, Y. Liang, H. Dong, X. Wang, Y. Yao, Charge storage mechanism of a quinone polymer electrode for zinc-ion batteries, J. Electrochem. Soc. 167 (2020), 070558.
[15] A. Nimkar, F. Malchick, B. Gavriel, M. Turgeman, G. Bergman, T. Fan, S. Bublil, R. Cohen, M. Weitman, N. Shpigel, M.D. Levi, D. Aurbach, Influences of cations' solvation on charge storage performance in polyimide anodes for aqueous multivalent ion batteries, ACS Energy Lett. 6 (2021) 2638–2644.
[16] Z. Song, Y. Qian, T. Zhang, M. Otani, H. Zhou, Poly(benzoquinonyl sulfide) as a high-energy organic cathode for rechargeable Li and Na batteries, Adv. Sci. 2 (2015) 1500124.
[17] G.S. Richard Boddy, Statistical Methods in Practice: for Scientists and Technologists, John Wiley & Sons, Ltd, 2009, pp. 92–94.
[18] J.L. Devore, Probability and Statistics for Engineering and the Sciences, Cengage Learning, Boston, 2015, pp. 357–359.
[19] I. Jureviciute, S. Bruckenstein, A.R. Hillman, Counter-ion specific effects on charge and solvent trapping in poly(vinylferrocene) films, J. Electroanal. Chem. 488 (2000) 73–81.
[20] N. Levy, M.D. Levi, D. Aurbach, R. Demadrille, A. Pron, Failure and stabilization mechanisms in multiply cycled conducting polymers for energy storage devices, J. Phys. Chem. C 114 (2010) 16823–16831.
[21] M.J.M. Jafeen, M.A. Careem, S. Skaarup, A study on the electrochemical behaviour of polypyrrole films in concentrated aqueous alkali halide electrolytes, Ionics 20 (2014) 535–544.
[22] J.N. Israelachvili, Intermolecular and Surface Forces, third ed., Academic Press, Academic Press, 2011, pp. 96–97.
[23] X.-B. Wang, J.B. Nicholas, L.-S. Wang, Electronic instability of isolated SO_4^{2-} and its solvation stabilization, J. Chem. Phys. 113 (2000) 10837–10840.
[24] J. Zhou, G. Santambrogio, M. Brümmer, D.T. Moore, L. Wöste, G. Meijer, D.M. Neumark, K.R. Asmis, Infrared spectroscopy of hydrated sulfate dianions, J. Chem. Phys. 125 (2006) 111102.
[25] M. Prakash, V. Subramanian, Ab initio and density functional theory (DFT) studies on triflic acid with water and protonated water clusters, J. Mol. Model. 22 (2016) 293.
[26] J. Stangret, T. Gampe, Ionic hydration behavior derived from infrared spectra in HDO, J. Phys. Chem. 106 (2002) 5393–5402.
[27] P.-Å. Bergström, J. Lindgren, An infrared spectroscopic study of the hydration of the triflate ion ($CF_3SO_3^-$) in aqueous solution, J. Mol. Struct. 239 (1990) 103–111.
[28] L. Jiang, Y. Lu, C. Zhao, L. Liu, J. Zhang, Q. Zhang, X. Shen, J. Zhao, X. Yu, H. Li, X. Huang, L. Chen, Y.-S. Hu, Building aqueous K-ion batteries for energy storage, Nat. Energy 4 (2019) 495–503.
[29] T. Ma, A.D. Easley, S. Wang, P. Flouda, J.L. Lutkenhaus, Mixed electron-ion-water transfer in macromolecular radicals for metal-free aqueous batteries, Cell Rep. Phys. Sci. 2 (2021) 100414.
[30] Y. Sun, N. Liu, Y. Cui, Promises and challenges of nanomaterials for lithium-based rechargeable batteries, Nat. Energy 1 (2016) 16071.
[31] Y. Shi, L. Peng, Y. Ding, Y. Zhao, G. Yu, Nanostructured conductive polymers for advanced energy storage, Chem. Soc. Rev. 44 (2015) 6684–6696.
[32] R. Zhan, X. Wang, Z. Chen, Z.W. Seh, L. Wang, Y. Sun, Promises and challenges of the practical implementation of prelithiation in lithium-ion batteries, Adv. Energy Mater. 11 (2021) 2101565.